sustainability

MDPI

*Article*

# Design Framework for Porous Mixture Containing 100% Sustainable Binder

**Genhe Zhang [1,2], Bo Ning [2], Feng Cao [2], Taotao Li [2], Siyuan Guo [1,*], Teng Gao [3], Biao Ma [1] and Rui Wu [4,*]**

[1] Key Laboratory for Special Area Highway Engineering of Ministry of Education, Chang'an University, Xi'an 710064, China
[2] China Communications Second Highway Engineering Bureau 7th Co., Ltd., Nanning 530220, China
[3] Xi'an Highway Survey and Design Institute Co., Ltd., Xi'an 710100, China
[4] Faculty of Civil Engineering and Geosciences, Delft University of Technology, 2628 CN Delft, The Netherlands
* Correspondence: 2021221268@chd.edu.cn (S.G.); r.wu-2@tudelft.nl (R.W.)

**Abstract**

This study developed a design framework for porous mixtures using a 100% sustainable non-bituminous epoxy–polyurethane binder system. Conventional design protocols for porous asphalt mixtures exhibit limitations in accurately controlling void content and mixture composition. This study proposed a novel design framework for porous mixtures containing 100% sustainable binder based on statistical analysis and theoretical calculations. The relationships among target air voids, binder content, and aggregate gradation were systematically analyzed, and calculation formulas for coarse aggregate, fine aggregate, and mineral filler contents were derived. A mix design framework was further established by applying the void-filling theory, where the combined volume of binder, fine aggregate, and filler equals the void volume of the coarse aggregate skeleton, thereby ensuring precise control of the target void ratio. Additionally, mixing procedures were investigated with emphasis on feeding sequence, compaction method, and mixing temperature. Results indicated that the optimized feeding sequence significantly improved binder distribution; specimens compacted using the Marshall double-sided compaction method achieved a density of 89.60%. Rheological analysis revealed that at 30 °C, the viscosities of sustainable binder and polyurethane filler were 1280 mPa·s and 6825 mPa·s, respectively, suggesting optimal mixture uniformity. The proposed methodology and process parameters provide essential technical guidance for engineering applications of porous mixtures containing 100% sustainable binder.

**Keywords:** porous pavement; mix design; epoxy resin mixture; target void ratio



Academic Editor: Antonio D'Andrea

Received: 27 November 2025
Revised: 27 December 2025
Accepted: 14 January 2026
Published: 19 January 2026



## 1. Introduction

Permeable Asphalt Concrete (PAC), with its typical void ratio of 18–22%, has been widely applied worldwide [1]. Its internal void structure provides excellent drainage, noise reduction, and skid resistance, making void content the most critical factor influencing performance [2]. However, PAC design in practice still relies heavily on empirical trial-and-error approaches and site-specific experiments, lacking a unified theoretical framework to balance functional and mechanical requirements. This limitation highlights the necessity of developing more rational mix design methodologies, while also providing a basis for considering epoxy-based porous mixtures as a promising long-life alternative.

The road sector faces the challenges of increasing binder demand in construction, energy-supply constraints, crude-oil price volatility, and the approach of net-zero targets;

the heavy non-renewable resource burden of bituminous materials underscores the urgent need for sustainable alternative binders [3–6]. Among these, epoxy-based systems have attracted attention for pavement applications due to their superior durability and substantially longer service life compared with conventional porous asphalt pavements [7]. These limitations in conventional PAC further highlight the need to explore sustainable binder alternatives.

Within PAC systems, gradation governs pore connectivity and skeleton stability. Image-based evaluations and void-filling/CAVF frameworks have linked sieve windows to connected voids and enabled target void designs with balanced functional and mechanical performance [8]. The fatigue behavior of porous asphalt mixtures has been a focal point of rigorous study among many scholars [9]. Equations were developed for the correlation between the fatigue behavior of asphalt binder and asphalt mixtures. Li et al. [10] investigated the tension–compression anisotropy of asphalt mixtures by employing dynamic modulus and fatigue tests under both compression and tension modes. Based on this, a fatigue damage characteristic curve was established, providing a reliable reference for evaluating the fatigue performance of asphalt mixtures. Nevertheless, these advances still rely on bituminous binders and remain sensitive to drain-down, moisture damage, and aging at high void ratios, which motivates the exploration of sustainable alternatives, particularly epoxy-based non-bituminous binders, and their integration into PAC. Epoxy resins are thermosetting polymers with strong adhesion; high mechanical strength; and excellent resistance to fatigue, deformation, and moisture, and they have been increasingly applied in porous asphalt systems. Recent studies have demonstrated that epoxy asphalt porous mixtures exhibit significantly improved fatigue performance, enhanced durability and aging resistance, and superior cracking and moisture damage resistance [11,12]. The sustainable partial-replacement route blends renewable or low-carbon modifiers with petroleum bitumen to improve performance. Recent studies have shown that lignin- or bio-oil-modified binders can partially substitute bitumen while maintaining comparable workability and improving ageing resistance and rutting performance [13,14]. In contrast, sustainable non-bituminous binders such as epoxy-based systems provide a full-replacement route, where sustainability is achieved through extended service life, reduced maintenance, and fewer distresses compared with conventional porous asphalt pavements [15–17].

Sustainable epoxy resin is a thermosetting polymer material that is widely used in electrical, electronic, and engineering fields [18,19]. Epoxy was initially employed as a modifier of petroleum bitumen, forming epoxy asphalt to enhance adhesion and moisture resistance at the pavement–steel interface of orthotropic steel bridge decks; building on this foundation, subsequent studies investigated the impact fatigue response and failure mechanisms of epoxy asphalt concrete to mitigate deck bumps and fatigue cracking. These studies have found that epoxy resin asphalt mixtures exhibit satisfactory strength characteristics, cracking resistance, moisture damage resistance, and strong deformation resistance. According to Liu et al. [20], a toughened epoxy asphalt binder synthesized from epoxy resin and 70# bitumen exhibited superior performance across multiple laboratory benchmarks. In 60 °C wheel tracking tests, mixtures with over 30% epoxy resin displayed a dynamic stability exceeding 20,000 passes/mm and a rutting depth under 1 mm, far outperforming standard regulatory benchmarks. Furthermore, at a 40% dosage, the mixture's moisture resistance was remarkably enhanced; the residual stability and tensile strength ratio (TSR) both remained above 90%, representing improvements of 15.2% and 15.5%, respectively, over non-modified counterparts. Xu et al. [21] investigated the strength characteristics of sustainable epoxy resin binders. Results showed that the uniaxial penetration strength of the sustainable epoxy mixture reached 3.5 MPa, substantially exceeding the 1.6 MPa maxi-

mum observed in conventional asphalt mixtures. Regarding flexural–tensile properties, the mixture maintained a strain exceeding 5342 με after 30 days of curing, outperforming traditional asphalt mixtures. Furthermore, predictive models for compressive and flexural–tensile strengths were proposed to facilitate further research. More importantly, full replacement of petroleum bitumen with epoxy-based binders enables a substantial extension of pavement service life, thereby reducing maintenance frequency and life-cycle costs. Studies have indicated that sustainable epoxy resin mixtures offer advantages such as enhanced rutting resistance, moisture damage resistance, low-temperature performance, fatigue resistance, and deformation coordination.

The performance of porous sustainable epoxy resin mixtures is governed by the mix-proportion design and mixing process. In practice, mix design relies heavily on empirical trial-and-error methods and site-specific experiments, leading to specific gradation selection and limited control of connected porosity. At the same time, research has also highlighted that mixture performance is highly sensitive to the mixing process. Factors such as the sequence of material addition, compaction method, and mixing temperature directly affect the distribution uniformity of the binder, the encapsulation effect of aggregates, and the overall homogeneity of the mixture. Improper control of the mixing process may lead to uneven binder distribution, insufficient compaction, and a decline in mechanical properties, thereby limiting its engineering application effectiveness. Therefore, it is essential to conduct a systematic study on the mixing process to clarify the relationship between key process parameters and performance. To address this, several studies have attempted to model and optimize the process. For example, Du et al. proposed a mixing kinetics model that considers temperature, volume, and method, showing high predictive accuracy after calibration with laboratory data [22]. Kisku et al. evaluated mechanical properties and ITZ microstructure using ten established mixing methods and a novel two-stage mixing approach, confirming the effect of the procedures on strength [23]. Li et al. compared conventional and alternative blending approaches for fiber dispersion and proposed an optimized method that improved flexural tensile strength by 40.6% with shorter mixing time [24]. These findings provide useful insights but remain fragmented, lacking an integrated framework that systematically couples proportioning design with process optimization.

It should be noted that the work reported in this paper is based on laboratory-controlled conditions; the effects of extreme temperatures and long-term field performance are beyond the scope of the present study. To address the problems of empirical mix design practices and the lack of systematic control over key process parameters, this study develops a target-void-based mix-proportioning framework for porous sustainable epoxy resin mixtures. In contrast to existing epoxy porous mixture design methods that largely transplant PAC gradations and adjust binder contents through trial and error, the proposed framework explicitly couples aggregate skeleton gradation; target void ratio; and the volumes of binder, fine aggregate, and filler through statistical regression and void-filling theory, and introduces a correction factor between target and measured void ratios to achieve controllable connected porosity for mixtures containing 100% sustainable epoxy binder. Furthermore, it investigates the effects of critical process variables, including feeding sequence, compaction method, and mixing temperature, on mixture performance to clarify the intrinsic relationships between process conditions and performance evolution. The results provide critical insights into mixture homogeneity, compaction efficiency, and mechanical stability, and the integrated design–process framework advances the scientific understanding of porous sustainable epoxy resin mixture design.

## 2. Materials and Methods

### *2.1. Theoretical Background*

The selection and properties of the binder are crucial for developing porous sustainable epoxy resin mixtures with enhanced mechanical properties and a high void content, which in turn ensures pavement performance and longevity. The binder for surface-layer epoxy resin pavements must meet specific engineering requirements. Prior to curing, it should have an appropriate initial viscosity for good workability. Once cured, it must possess sufficient mechanical strength and low-temperature relaxation to maintain the mixture's in-service performance. Furthermore, the open-to-traffic time is a key consideration, primarily influenced by the binder's curing times. In this section, we optimized the binder for porous sustainable epoxy resin mixtures based on these specific service requirements. Using orthogonal experimental data, we determined the optimal proportions of modified sustainable epoxy resin, curing agent, diluent, and accelerator by establishing criteria for curing times.

### *2.2. Test Protocol and Mix-Proportion Determination*

A Taguchi-based orthogonal experimental design was adopted to screen the effects of four formulation factors on multiple responses [25] (viscosity, tensile strength, and elongation at break). Range analysis and analysis of variance (ANOVA) were performed to quantify factor significance, and a multi-response desirability approach was employed to identify a balanced formulation satisfying workability and early-age mechanical requirements. The sustainable epoxy resin content was fixed at 100%, while the proportions of toughening agent, diluent, curing agent, and accelerator, relative to the sustainable epoxy resin, were systematically varied. The investigated factor levels were selected based on preliminary trials and construction-driven constraints: the lower bounds were set to avoid incomplete curing, whereas the upper bounds were limited to prevent overly rapid gelation and insufficient compaction time. In particular, the ranges of the curing agent and accelerator were chosen to provide a workable pot life and allow early opening to traffic under laboratory-controlled mixing and molding conditions. To characterize the rheological and mechanical performance, the viscosity was first determined via a Brookfield rotational viscometer at 25 °C. Tensile properties were assessed using standard dumbbell-shaped specimens (GB/T 2567-2021) [26], which were cured to maturity and measured on an MTS universal testing system. During the tensile test, an extensometer was employed to capture the real-time elongation of the 50 mm gauge section to calculate the fracture strain. Viscosity serves as a vital parameter for assessing the construction workability of sustainable epoxy resin. An optimal viscosity range is essential: a low value results in inadequate aggregate coating, while an overly high viscosity hinders the attainment of a homogeneous mixture during blending. This approach was used to investigate the effects of these four components on the performance of the sustainable epoxy resin binder. The results of the orthogonal experiment are shown in Table 1.

**Table 1.** Results of the experimental evaluation indices.

| Number \ Factor | Toughening Agent (%) | Diluent (%) | Curing Agent (%) | Accelerator (%) | Viscosity (mPa·s) | Tensile Strength (MPa) | Elongation at Break (%) |
|---|---|---|---|---|---|---|---|
| 1 | 5 | 40 | 40 | 3.0 | 1105 | 18.84 | 0.69 |
| 2 | 5 | 45 | 45 | 3.5 | 851 | 20.84 | 2.88 |
| 3 | 5 | 50 | 50 | 4.0 | 745 | 22.52 | 73.53 |
| 4 | 5 | 55 | 55 | 4.5 | 618 | 25.58 | 84.68 |
| 5 | 5 | 60 | 60 | 5.0 | 502 | 27.29 | 89.47 |
| 6 | 10 | 40 | 45 | 4.0 | 1330 | 25.98 | 1.02 |
| 7 | 10 | 45 | 50 | 4.5 | 1012 | 28.53 | 3.34 |
| 8 | 10 | 50 | 55 | 5.0 | 880 | 32.51 | 61.38 |
| 9 | 10 | 55 | 60 | 3.0 | 696 | 21.12 | 104.09 |
| 10 | 10 | 60 | 40 | 3.5 | 782 | 9.02 | 128.22 |
| 11 | 15 | 40 | 50 | 5.0 | 1386 | 32.53 | 0.42 |
| 12 | 15 | 45 | 55 | 3.0 | 1148 | 25.06 | 5.22 |
| 13 | 15 | 50 | 60 | 3.5 | 1138 | 29.31 | 89.67 |
| 14 | 15 | 55 | 40 | 4.0 | 1240 | 18.48 | 104.92 |
| 15 | 15 | 60 | 45 | 4.5 | 1095 | 20.33 | 110.25 |
| 16 | 20 | 40 | 55 | 3.5 | 1898 | 39.57 | 3.46 |
| 17 | 20 | 45 | 60 | 4.0 | 1510 | 43.06 | 7.96 |
| 18 | 20 | 50 | 40 | 4.5 | 1610 | 21.27 | 72.80 |
| 19 | 20 | 55 | 45 | 5.0 | 1363 | 24.21 | 103.26 |
| 20 | 20 | 60 | 50 | 3.0 | 1262 | 11.05 | 154.24 |
| 21 | 25 | 40 | 60 | 4.5 | 2092 | 43.73 | 5.22 |
| 22 | 25 | 45 | 40 | 5.0 | 2413 | 28.81 | 7.84 |
| 23 | 25 | 50 | 45 | 3.0 | 2010 | 13.68 | 144.38 |
| 24 | 25 | 55 | 50 | 3.5 | 1760 | 15.40 | 152.56 |
| 25 | 25 | 60 | 55 | 4.0 | 1388 | 17.66 | 145.32 |

The orthogonal experimental data indicated that the proportions of individual components directly determined the properties of the cured epoxy resin binder. The primary factors affecting viscosity were, in order, diluent, curing agent, and accelerator; for tensile strength, the order of influence was diluent, curing agent, and accelerator; and for elongation at break, the order was diluent, accelerator, and curing agent. Considering the application requirements of the binder, including an appropriate initial viscosity, sufficient post-curing strength, and toughness, the ratio of sustainable epoxy resin to toughening agent was set at 7:2. The selected amounts were 120 parts of modified sustainable epoxy resin, 65 parts of diluent, 35–55 parts of curing agent, and 1.5–5.0 parts of accelerator.

To further determine the optimal proportions of the curing agent and accelerator, the gelation and curing times of binders with varying component ratios were measured. Gelation time was defined as the period from the initiation of the chemical reaction within the sustainable epoxy resin system until it lost its flowability. Curing time was defined as the duration from the point of gelation until the system developed sufficient post-cure strength. The experimental results are summarized in Table 2.

**Table 2.** Gelation and curing times at different mix proportions.

| No. | Modified Sustainable Epoxy Resin | Diluent | Curing Agent | Accelerator | Gel Time | Curing Time |
|---|---|---|---|---|---|---|
| 1 | 120 | 65 | 35 | 1.5 | 63 | uncured |
| 2 | 120 | 65 | 45 | 1.5 | 70 | 40 |
| 3 | 120 | 65 | 55 | 1.5 | 75 | 45 |
| 4 | 120 | 65 | 45 | 2.0 | 53 | 34 |
| 5 | 120 | 65 | 45 | 2.5 | 49 | 26 |
| 6 | 120 | 65 | 45 | 3.0 | 49 | 20 |
| 7 | 120 | 65 | 45 | 4.0 | 33 | 30 |
| 8 | 120 | 65 | 45 | 5.0 | 26 | 21 |

When the amount of curing agent exceeded 45 parts, the binder could successfully cure, and further increases had negligible effects on extending gelation and curing times. Therefore, the curing agent content was set at 45 parts. As the accelerator content increased, the overall molding time of the road-use sustainable epoxy resin binder showed a decreasing trend. For a binder containing 3.0 parts of accelerator, the gelation and curing times were 49 min and 20 min, respectively. The gelation time was appropriate, and the curing time was minimal. The total molding time exceeded 1 h, meeting the construction and open-to-traffic requirements for porous sustainable epoxy resin mixtures.

### *2.3. Sustainable Binder*

The sustainable binder is a synthesis composite, comprising bisphenol A-type sustainable epoxy resin as the primary agent sustainable binder, and polyurethane prepolymer as the toughening modifier. The mass ratio of sustainable epoxy resin to toughening agent was 7:2. Polysulfide thiol was used as the curing agent, polyethylene glycol diglyceryl ether was employed as the diluent, and DMP-30 was employed as the accelerator. As indicated by the orthogonal test results in Tables 1 and 2, the formulation listed in Table 3 was adopted as the final binder composition because it provided an appropriate initial viscosity (2500 mPa·s) and favorable tensile strength (22.4 MPa) and elongation at break (18.2%), thereby balancing construction workability and mechanical performance. For this formulation, the gelation and curing times are approximately 49 min and 20 min, respectively, which ensure sufficient molding/compaction time during construction while still satisfying the requirement of early opening to traffic for porous sustainable epoxy resin mixtures.

**Table 3.** Composition of road-grade sustainable binder.

| Modified Sustainable Epoxy Resin | Diluent | Curing Agent | Accelerator |
|---|---|---|---|
| 120 | 65 | 45 | 3.0 |

### *2.4. Preparation of Sustainable Binder*

Firstly, the sustainable epoxy resin was modified by thoroughly mixing it with the toughening agent in the specified proportion. After the sustainable epoxy resin mixture was homogeneously blended, the mixing container was placed in a vacuum-drying oven at a constant temperature of 25 °C for vacuum treatment until all air bubbles in the mixture were eliminated, forming the road-grade sustainable binder.

### *2.5. Aggregates*

Coarse Aggregates

The morphological characteristics of aggregates have a significant impact on the physical and mechanical properties of the mixture and the distribution of the void structure [27]. In this study, limestones were selected as the coarse and fine aggregates, and limestone powder was selected as the mineral filler to prepare the porous bio-mixtures.

### *2.6. Test Methods for Mixtures*

#### 2.6.1. Determination of Void Ratio

Given that the target void ratio of the porous epoxy resin mixture is 18–26%, the material contains a substantial internal void structure. For mixtures of this type, the void ratio is generally determined by the volumetric method or the vacuum sealing method. The volumetric method is simple to perform but prone to larger errors, whereas the vacuum sealing method yields data with smaller fluctuations and lower errors, closer to the actual value. Accordingly, with reference to the Specification for Design and Construction of

Porous Asphalt Pavements, this study determines the void ratio of the porous epoxy resin mixture using the vacuum sealing method.

#### 2.6.2. Abrasion Resistance Testing

The abrasion test was conducted using standard Marshall specimens compacted by 50 blows per face, with a specimen height of 63.5 mm ± 1.3 mm. A molded porous epoxy resin mixture specimen was placed in a Los Angeles abrasion machine (Matest, Treviolo, Italy) and rotated for 300 revolutions at 30–33 r/min. The abrasion loss mass was obtained by subtracting the mass of the largest remaining piece from the original mass of the mixture.

#### 2.6.3. Penetration Testing

The material's permeability was quantified by measuring its hydraulic conductivity (k) with a constant head permeameter. The test procedure was as follows: (1) Marshall specimens of the porous epoxy resin mixture were prepared following the mix design and, after curing, were kept in the mold. A cylindrical sleeve was mounted on the top, and rubber tape was wrapped between the sleeve and the mold to ensure a watertight seal. (2) Water was supplied into the sleeve from an external source, and the valve was adjusted until the overflow orifice maintained a constant head. (3) With the head held constantly, water percolated downward through the specimen. The effluent was collected in a graduated cylinder, and the volume transmitted over approximately 5 s was recorded.

#### 2.6.4. Mechanical Property Testing

(1) Uniaxial compression

Cylindrical specimens (φ100 mm × 100 mm) prepared by static compaction were conditioned in an oven at 15 °C for 12 h. Following the uniaxial compression procedure in the Test Specifications for Asphalt and Asphalt Mixtures in Highway Engineering, we determined the compressive strength and resilient modulus for mixtures with different target voids and binder dosages.

(2) Splitting (indirect tensile) strength testing

Marshall specimens were tested in splitting tension using arc-shaped loading strips of specified width until failure; the splitting tensile strength (indirect tensile strength, ITS) was computed to evaluate mechanical performance. Test parameters were as follows: 15 °C ± 0.5 °C and 50 mm/min loading rate.

#### 2.6.5. High-Temperature Stability Testing

Assessment of the high-temperature stability for conventional porous asphalt mixtures is typically conducted using the 60 °C rutting test. For the porous epoxy resin mixtures investigated in this study, the requirements specified in the Standard Test Methods of Bitumen and Bituminous Mixtures for Highway Engineering (JTG 3410-2025) [28] can be referenced. Specifically, the porous epoxy resin mixture specimens are compacted into 300 mm × 300 mm × 50 mm slabs for the rutting test. The testing environment is maintained at 60 °C. A solid rubber wheel, applying a wheel load of 0.7 MPa, is employed to repeatedly roll over the specimen along the same track, inducing a permanent deformation known as a rut. The rutting resistance of the porous epoxy resin mixture is subsequently evaluated by measuring the Rut Depth (RD, in mm) and the dynamic stability (DS, in cycles).

#### 2.6.6. Resistance to Low-Temperature Cracking Test

The low-temperature stability of the porous epoxy resin mixtures was evaluated using the low-temperature splitting test. The experimental procedure was analogous to the

previously described splitting test, but with modified test parameters. Specifically, the test was conducted at a controlled temperature of −10 ± 0.5 °C and a loading rate of 1 mm/min.

## 3. Analysis of the Target Void Ratio and Aggregate Gradation Distribution of Porous Asphalt Mixture

### *3.1. Distribution Properties of Aggregate Gradation Composition in Porous Asphalt Mixture*

In this study, PAC-13 was taken as the research subject. A total of 100 sets of aggregate gradation compositions were screened and compiled. The data were processed using the Pauta criterion (3σ rule) to eliminate outliers, resulting in 21 valid gradation sets, as shown in Figure 1 [29].

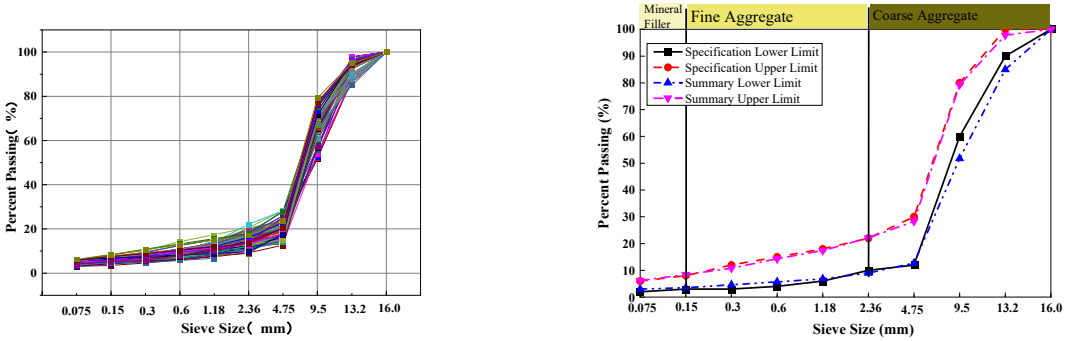


(**a**) Effective grading composition from the literature (**b**) Comparison between effective grading compositions

**Figure 1.** Summary of PAC-13 grading composition.

From Figure 1, it can be observed that the effective gradation composition range of AC-13 is similar to the PAC-13 gradation range in specifications. The upper gradation limit is almost identical, but there are some minor differences in the lower gradation limits. Using the passing rate through the 2.36–4.75 mm sieve as the boundary, the passing rate of fine aggregates below the 2.36–4.75 mm sieve is slightly higher than that of the lower limit of the specification gradation, while the passing rate of coarse aggregates above the 2.36–4.75 mm sieve is slightly lower than the lower limit of the specification gradation.

To further analyze the distribution of aggregate gradations, Figures 2–4 show the distribution of passing percentages for coarse aggregate, fine aggregate, and mineral filler, respectively, at each sieve size within the PAC-13 gradation statistical samples.

Based on Figure 2, varying conclusions and recommendations were reached regarding the proportion of the coarse aggregate size fraction and its effect on mixture's performance. The 9.5 mm particles were the main particles forming the coarse aggregate skeleton and significantly impacted the structure of the coarse aggregate skeleton and the void structure of the mixture. Furthermore, the passing rates for the 4.75 mm and 2.36 mm sieves had a significant impact on the void ratio of the porous asphalt mixture. Therefore, variations in the passing rates and their effects should be clearly defined and strictly controlled.

As illustrated in Figure 3, conventional porous asphalt mixtures contain a very low proportion of fine aggregate. The distribution of fine aggregate passing percentages for each sieve is concentrated in a range around and below the specified median. An excessive proportion of fine aggregate results in a substantial reduction in void content, thereby failing to satisfy the specifications for draining and noise-reducing pavements.

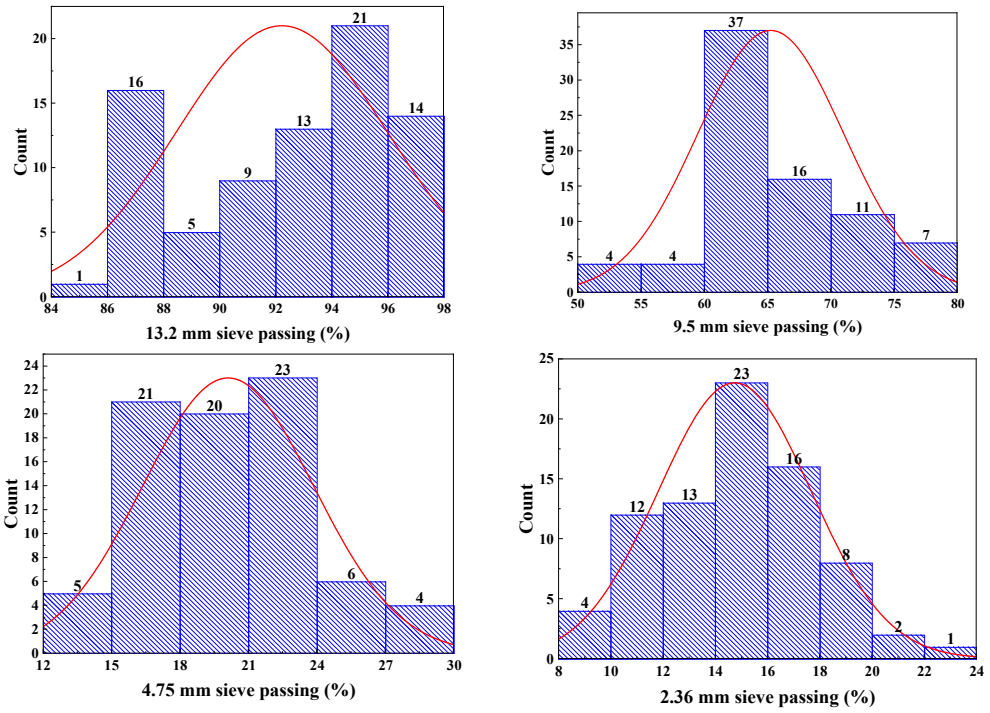


**Figure 2.** Distribution of coarse aggregate sizes.

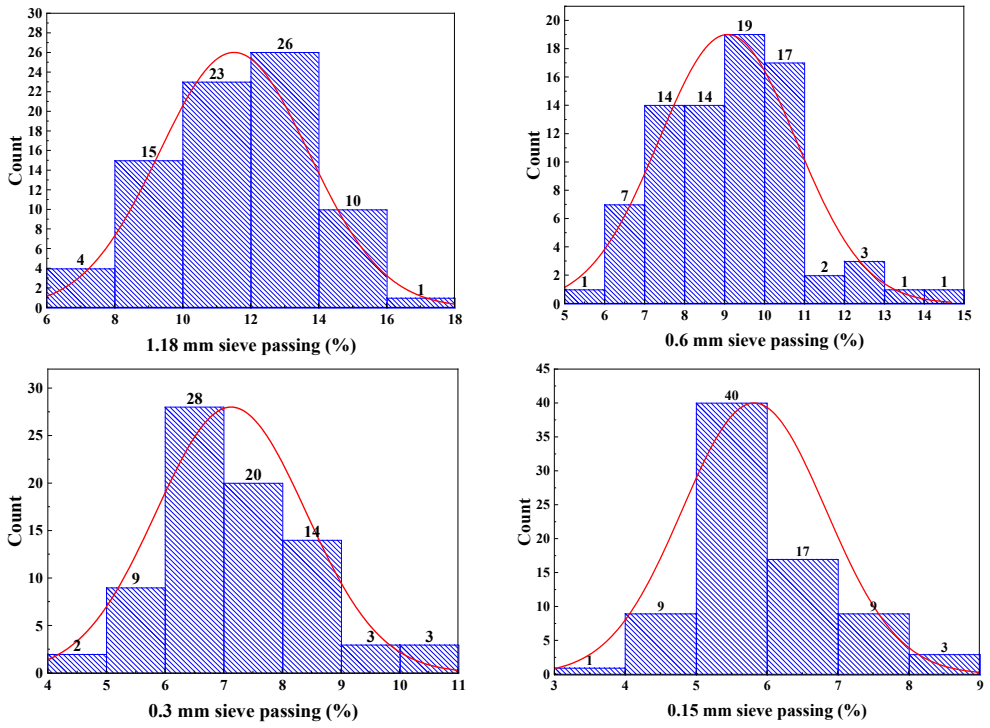


**Figure 3.** Distribution of fine aggregate passing percentages.

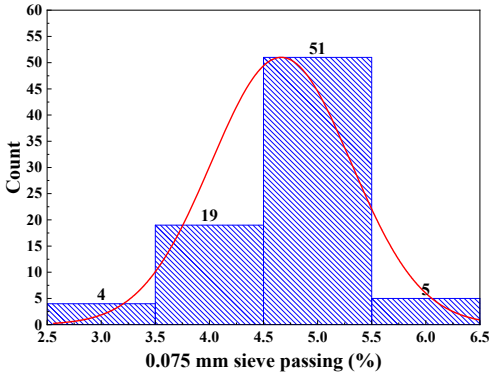


**Figure 4.** Distribution patterns of mineral powder.

Based on Figure 4, the mineral filler content in conventional porous asphalt mixtures exhibits a range of 4%. Over half of the studies included in this analysis utilized a mineral filler content concentrated between 4.5% and 5.5%.

### *3.2. Analysis of the Relationship Between Sieve Passing Rate and Porosity of Mineral Aggregates*

To statistically analyze the correlation between the passing percentages at various sizes and the void content of the mixture, fitting analysis of the relationship between the porosity of the mixture and the sieve passing rates at different sieve sizes was performed using Origin software (Origin Pro 2025), and the results are shown in Figure 5.

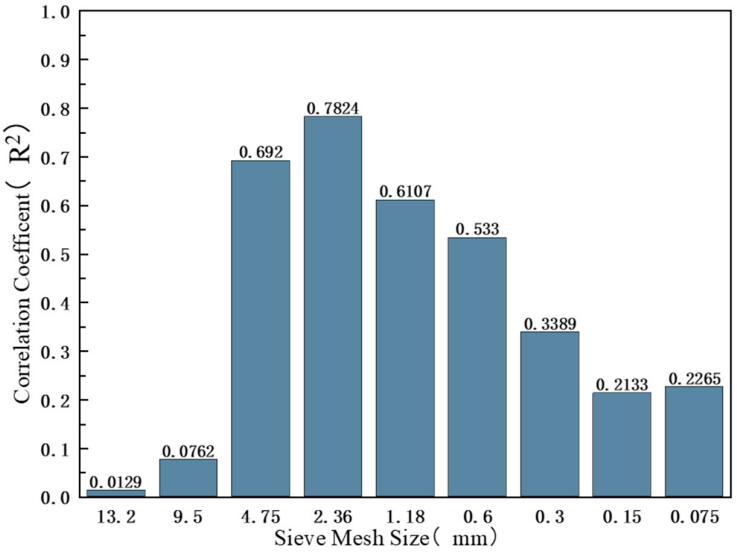


**Figure 5.** Correlation between Sieve Mesh Passing Rate and Mixture Porosity.

From Figure 5, it can be observed that the 2.36 mm sieve, which serves as the boundary between coarse and fine aggregates, shows the most significant correlation with porosity, with an $R_{2.36}{}^2$ of 0.78239. The $P_{4.75\,mm}$ exhibits the second-strongest correlation with porosity, with an $R_{4.75}{}^2$ of 0.61069. Therefore, it is crucial to focus on controlling the passing rates of the 2.36 mm and 4.75 mm sieves when designing the mixture proportions.

## 4. The Method for Determining the Standard Mix Proportion of Sustainable Epoxy Mixture

Based on the target porosity of the porous mixture and the aggregate gradation distribution law outlined in Section 3.1, this study establishes the relationship between the passing rate of sieve sizes above 2.36 mm and the target porosity of the mixture. It

quantitatively characterizes the impact of the coarse aggregate content above 2.36 mm on the aggregate structure and porosity structure of the mixture. Drawing on the 'reserved porosity' concept, the functional air-void fraction is predefined at the mix design stage to be retained so that, after construction compaction and subsequent in-service densification, the mixture's effective porosity still meets the design target. A standard mix-design method for porous sustainable epoxy resin mixtures combining theoretical calculations with laboratory testing was developed. Specifically, (i) the packing relationships among aggregate size fractions were identified through statistical analysis; (ii) the voids in mineral aggregate (VMA) were determined from interlock–packing tests; and (iii) by controlling the target air-void content, the binder content, fine aggregate dosage, and baseline mix proportions are obtained. The calculation workflow is shown in Figure 6.

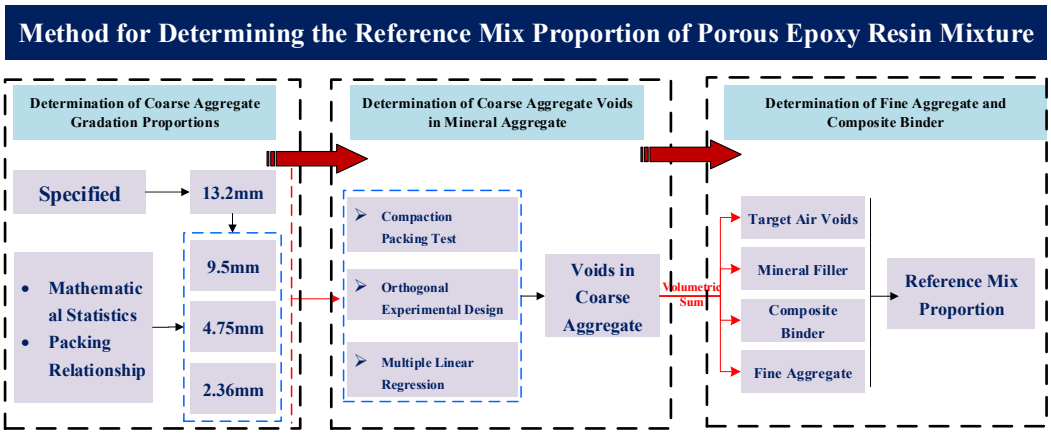


**Figure 6.** Calculation and determination method for mix proportion of porous sustainable epoxy resin mixture.

### *4.1. Determination of Target Porosity*

The requirements for the target porosity of drainage pavements in the United States, Europe, Japan, and other regions are shown in Table 4.

**Table 4.** Requirements for porosity of drainage pavements worldwide.

| | Country and Organization Name | Porosity Range/% |
|---|---|---|
| United States | National Asphalt Pavement Association [30] | >18 |
| | Texas Department of Transportation [31] | 18~22 |
| | Federal Highway Administration [32] | 15 |
| Japan | | 20 |
| Netherlands | | >20 |
| Italy | | 18~23 |
| Spain | | >20 |

From Table 4, it can be observed that the commonly used porosity for PAC pavements ranges from 18% to 22%. Based on the actual rainfall statistics from various regions in China, relevant analyses and studies have been conducted on the design requirements for the target porosity of drainage pavements, and the results are shown in Table 5.

**Table 5.** Requirements of different rainfall intensities on void ratio [33].

| Rainfall Level | Rainfall Amount/(mm·h$^{-1}$) | Permeability Coefficient/(mm·s$^{-1}$) | Porosity/% |
|---|---|---|---|
| Light Rain | ≤2.5 | -- | -- |
| Moderate Rain | 2.6~8 | 0.14~0.44 | 14.1~18.6 |
| Heavy Rain | 8.1~16 | 0.45~0.83 | 18.7~21.6 |
| Torrential Rain | ≥16 | ≥0.89 | ≥22 |

Integrating Tables 4 and 5, we adopted 18–26% as the target porosity band: 18–24% (inclusive) is defined as a large-void sustainable epoxy resin mixture, and 24–26% as an ultra-large-void sustainable epoxy resin mixture. Although previous studies have reported that porous asphalt can be designed with porosities approaching ~28% while still meeting basic mechanical requirements [34], we did not directly adopt 28% as the upper limit. Instead, a slightly lower value of 26% was chosen as a conservative upper bound, considering that higher void ratios tend to aggravate raveling and abrasion loss, increase the sensitivity to construction variability in the field void ratio, and compromise long-term durability and structural safety, while 26% still ensures sufficient drainage capacity under the designed rainfall conditions.

### *4.2. Relationship Between Coarse Aggregate Dosage and Target Porosity of the Mixture*

This study focuses on PAC-13, with four types of coarse aggregates: 13.2 mm, 9.5 mm, 4.75 mm, and 2.36 mm. These aggregates form a skeletal pore structure through interlocking and filling. Drawing on prior research and the stepwise volume filling theory, Ghuzlan [35] investigated the interlocking effects of multi-sized particles. She identified distinct correlations between coarse aggregate sizes of 13.2 mm, 9.5 mm, 4.75 mm, and 2.34 mm. Grounded in these particle functions and previously validated findings, previous research has demonstrated that [36], under a given target porosity (*vv*) and a sieve residue corresponding to the 13.2 mm sieve, mathematical statistical methods can be used to derive relational Equations (1)–(3) between the gradation fractions and the 13.2 mm sieve residue. On this basis, the dosage proportions of the 9.5 mm, 4.75 mm, and 2.36 mm coarse aggregates can be further determined.

$$A_{9.5} = 40.22719 \bullet {A_{13.2}}^{-0.22435} \; R^2 = 0.931, \tag{1}$$

$$A_{4.75} = 170.8763 \bullet (A_{13.2} + A_{9.5})^{-0.37481} \; R^2 = 0.959, \tag{2}$$

$$A_{13.2} + A_{9.5} + A_{4.75} + A_{236} = 66.12763 + 0.9274\nu\nu \; R^2 = 0.667. \tag{3}$$

where $A_{13.2}$, $A_{9.5}$, $A_{4.75}$, and $A_{2.36}$ represent the sieve residue for the 13.2 mm, 9.5 mm, 4.75 mm, and 2.36 mm sieve fractions, respectively.

### *4.3. Determining the Correlation Between Porosity and Coarse Aggregate Materials*

To understand the influence of the sieve residue for the 13.2 mm, 9.5 mm, 4.75 mm, and 2.36 mm coarse aggregates on the coarse aggregate material porosity *VCA**, the sieve residue of each fraction was treated as a variable. Within the statistical range of each fraction, different sieve residue levels were selected and combined. Compaction tests were then carried out using a vibrating table compactor for these combinations. Finally, the results were analyzed by curve regression to establish Equation (4), which relates the material porosity to the sieve residue of each coarse aggregate fraction.

$$VCA^* = VV^0 = 8.0542A_{13.2}^{-0.01783} + 1.3633A_{9.5}^{0.019423} + 25.482A_{4.75}^{0.040716} - 2.8407A_{2.36}^{0.63802} \tag{4}$$

The correlation coefficient of the regression formula is $R^2$ = 0.901. This indicates that regression Formula (4) can accurately express the relationship between the material porosity and the different fractions of coarse aggregates.

### *4.4. Determining the Amount of Mineral Powder*

#### 4.4.1. Coarse Aggregate Specific Surface Area

The sustainable epoxy mixture consists of more than 80% coarse aggregates and a small amount of fine aggregates, mineral powder, and mixed binders. This study assumes that the material is primarily composed of coarse aggregates with a size of 2.36 mm and above, with the sustainable epoxy binder and mineral powder forming a uniform layer wrapped around the exterior of the coarse aggregates, as shown in Figure 7.

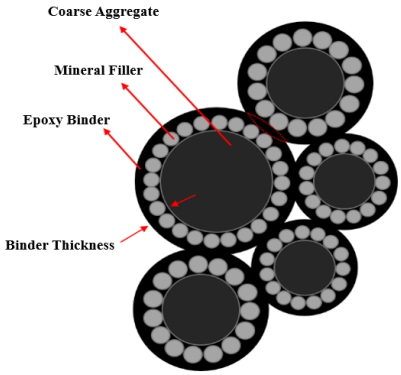


**Figure 7.** Schematic of sustainable-epoxy-binder- and mineral-powder-wrapped coarse aggregate.

To calculate the amount of mineral powder, the specific surface area (A) of the coarse aggregates must be obtained by the mineral surface area calculation formula provided by the National Asphalt Pavement Association MA-2 [17], as shown in Equation (5)

$$A = 0.41 + 0.41a + 0.82b + 1.64c + 2.87d + 6.14e + 12.29f + 32.77g \quad (5)$$

The variables $a$, $b$, $c$, $d$, $e$, $f$, and $g$ represent the cumulative mass percentages of aggregates passing through the sieves smaller than 4.75 mm. Since this study only considers coarse aggregates ≥2.36 mm, the fractions finer than 2.36 mm are treated separately as mineral powder, and therefore the values for c, d, e, f, and g are all taken as 0.

The results for the specific surface areas of the coarse aggregates are shown in Table 6.

**Table 6.** Calculation results of specific surface area of coarse aggregate.

| Target Porosity Range | Sieve Size/mm | | | | Specific Surface Area/(kg·m$^{-2}$) |
|---|---|---|---|---|---|
| | $A_{13.2}$ | $A_{9.5}$ | $A_{4.75}$ | $A_{2.36}$ | |
| 18%~24% | 5.0 | 28.0 | 46.0 | 5.6 | 0.645 |
| 24%~26% | 5.0 | 35.0 | 48.0 | 2.0 | 0.623 |

#### 4.4.2. Theoretical Calculation of Mineral Powder Usage

Based on aggregate packing theory [18], the mineral powder is simplified as spherical particles with an average particle size of $D_{MP}$. Assuming the particle size of the mineral powder d is 0.075 mm, the mineral powder usage is calculated for target porosity ranges of 18%~24% and 24%~26%. The results are shown in Table 7.

**Table 7.** Calculation results of mineral powder consumption.

| Target Porosity Range | $S_{ca}$/cm$^2$ | $N_T$/Number | $V_{MP}$/cm$^2$ | $m_{MP}$/g | $A_{MP}$/% |
|---|---|---|---|---|---|
| 18~24% | 6549.74 | 370,670 | 8.19 | 22.4 | 2.15% |
| 24~26% | 6732.56 | 380,903 | 8.41 | 23.0 | 2.08% |

### *4.5. Determination of Fine Aggregate and Binder Content*

In this study, filler refers to the materials used to fill the voids in the compacted skeleton of coarse aggregates, excluding the target voids. This includes fine aggregates, mineral powder, and mixed binder [37]. The related formulas are shown in Equations (6) and (7). Based on these formulas, the quantities of binder and fine aggregates can be derived.

$$V_{\text{Fill}} = (VCA^* - vv) \times V_{\text{CA}} \tag{6}$$

$$V_{\text{FILL}} = (VCA^* - vv) \times V_{\text{CA}} = \frac{m_{\text{FA}}}{\rho_{\text{FA}}} + \frac{m_{\text{MP}}}{\rho_{MP}} + \frac{m_{\text{binder}}}{\rho_{\text{binder}}} \tag{7}$$

where $V_{FILL}$ represents the volume of coarse aggregate mineral material required to fill the target voids, in cm$^3$; $V_{CA}$, $V_{FA}$, $V_{MP}$, and $V_{binder}$ represent the volumes of coarse aggregate, fine aggregate, mineral powder, and mixed binder, respectively, in cm$^3$; and $vv$ is the target void ratio, in %.

### *4.6. Correction of Target Void Ratio*

Through Marshall specimen preparation and volumetric analysis, the measured void ratios of the porous sustainable epoxy resin mixtures were tested under different mixed binder contents (3.0%, 3.5%, 4.0%, 4.5%, 5.0%) and different target void ratios (18%, 20%, 22%, 24%, 26%). The results are shown in Figure 8.

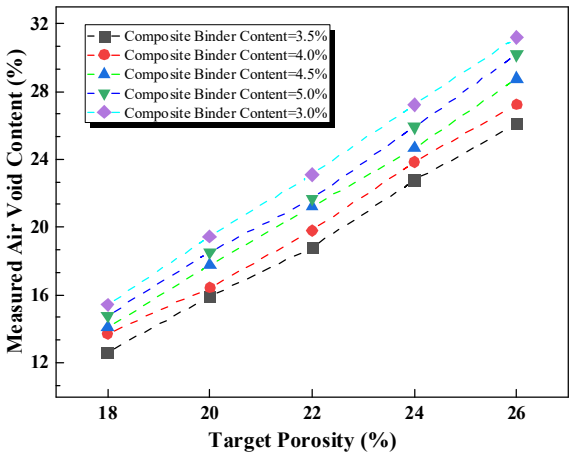


**Figure 8.** Relationship between measured voids and target voids.

From Figure 8, there is a certain deviation between the measured void ratio and the target void ratio, but there is a correlation between the two. Therefore, the target void ratio is corrected, and the corrected target void ratio $vv'$ is introduced. The relationship between the target void ratio $vv$ and the corrected target void ratio $vv'$ is shown in Equation (8).

$$vv' = \frac{vv}{k} \tag{8}$$

$$k = -3.31 + 4.4079 \times G_b^{-0.10658} + 121.4 \times vv^{-1.7462} \tag{9}$$

where $k$ is the correction factor and $G_b$ represents the mixed binder content, in %. In this paper, the filler refers to the volume of coarse aggregate material used to fill the voids, which includes fine aggregate, mineral powder, and mixed binder. The relationship is expressed in Equation (10).

$$V_{\mathrm{FILL}} = \left(VCA^* - \nu\nu'\right) \times V_{\mathrm{CA}} = \frac{m_{\mathrm{FA}}}{\rho_{\mathrm{FA}}} + \frac{m_{\mathrm{MP}}}{\rho_{\mathrm{MP}}} + \frac{m_{\mathrm{binder}}}{\rho_{\mathrm{binder}}} \quad (10)$$

where $V_{CA}$ is the volume of coarse aggregate material and $VCA^*$ is the void ratio of the coarse aggregate material. Based on Equations (8) and (9), the amount of mixed binder and fine aggregate can be derived, and the corrected reference mix ratio for the porous sustainable epoxy resin mixture can be obtained.

## 5. Case Study

In this case study, the target void ratio $vv$ is set to 20% and the binder volume Gb is taken as 3.0% (corresponding to Step 1 in Figure 8). According to the correction factor formula, the corrected target void ratio $vv$ and the corresponding correction factor k for different binder contents are then calculated (Step 2), and the results are summarized in Table 8. In the subsequent steps, $vv'$ is used to determine the coarse aggregate skeleton gradation and to compute the required volumes of binder, fine aggregate, and filler, which are finally converted into the mass proportions of each component in the designed porous sustainable epoxy resin mixture.

**Table 8.** Corrected results of target void ratio ($vv$) of 20%.

| Target Void Ratio ($vv$)/% | Binder Content/% | Correction Factor | Corrected Target Void Ratio ($vv'$)/% |
|---|---|---|---|
| 20 | 3.0 | 1.18 | 16.90 |
| | 3.5 | 1.13 | 17.64 |
| | 4.0 | 1.07 | 18.76 |
| | 4.5 | 1.02 | 19.57 |
| | 5.0 | 0.97 | 20.67 |

With a target void ratio of 20% and a binder content of 3.0%, the corrected target void ratio of 16.90% is calculated, using Table 8 as an example. Given that the sieve residue percentage for the 13.2 mm sieve is 5% and the total mass of the mineral material is 1200 g, PAC-13 is selected as the research object in this study, with a maximum nominal particle size of 13.2 mm. The sieve residue percentage for the 13.2 mm sieve is given as 5%. Using statistical Formulas (1)–(3), the quantities for the 9.5 mm, 4.75 mm, and 2.36 mm fractions are calculated in Table 9.

**Table 9.** Coarse aggregate usage by size (%).

| sieve size (mm) | 9.5 | 4.75 | 2.36 |
|---|---|---|---|
| aggregate content (%) | 28.04 | 81.80 | 2.70 |

The coarse aggregate material void ratio can be calculated as 35.19%. The quantities of filler, fine aggregate, and binder are calculated, as shown in Table 10.

**Table 10.** Calculation results.

| | |
|---|---|
| Coarse Aggregate Mass | 981.6 g |
| Apparent Bulk Density of Coarse Aggregate | 2.74 g/cm$^3$ |
| Compacted Bulk Density of Coarse Aggregate | 1.77 g/cm$^3$ |
| Void Volume of Coarse Aggregate Material | 553.18 cm$^3$ |

Required volume of fine aggregate, mineral powder, and binder mixture:

$$V_{\mathrm{FILL}} = \left(VCA^{*} - \nu\nu'\right) \times V_{\mathrm{CA}} = 101.19\ \mathrm{cm}^3$$

Furthermore, based on the engineering experience formula and theoretical calculation results, the mineral powder content in the gradation composition of the porous sustainable epoxy resin mixture in this study is selected to be 2.1%, with the given binder quantities being 3.0%. The fine aggregate amounts for different binder quantities are calculated using Equation (11).

$$m_{\mathrm{FA}} = \left(V_{\mathrm{FILL}} - \frac{m_{\mathrm{MP}}}{\rho_{\mathrm{MP}} - \frac{m_{\mathrm{binder}}}{\rho_{\mathrm{binder}}}}\right) \times \rho_{\mathrm{FA}} = 160.0\ \mathrm{g} \quad (11)$$

Similarly, the reference mix proportions of the porous epoxy resin mixture were calculated for target void ratios of 18%, 20%, 22%, 24%, and 26%, corresponding to binder contents of 3.0%, 3.5%, 4.0%, 4.5%, and 5.0%, respectively, as presented in Table 11.

**Table 11.** Basic mix proportion of sustainable porous epoxy resin mixture with different target voids.

| Target Void Ratio/% | Dosage of Mixed Binder/% | Passing Rate Through Each Sieve Mesh/% | | | | |
|---|---|---|---|---|---|---|
| | | 13.2 | 9.5 | 4.75 | 2.36 | 0~1.18 |
| 18 | 3.0 | 95.05 | 67.28 | 21.66 | 21.50 | 2.08 |
| | 3.5 | 94.90 | 66.29 | 19.27 | 18.42 | 2.62 |
| | 4.0 | 94.78 | 65.52 | 17.44 | 15.71 | 2.19 |
| | 4.5 | 94.68 | 64.88 | 15.92 | 13.49 | 2.23 |
| | 5.0 | 94.58 | 64.20 | 14.29 | 10.90 | 2.28 |
| 20 | 3.0 | 94.86 | 66.03 | 18.65 | 15.87 | 2.16 |
| | 3.5 | 94.77 | 65.44 | 17.26 | 13.71 | 2.39 |
| | 4.0 | 94.67 | 64.78 | 15.67 | 10.95 | 2.24 |
| | 4.5 | 94.58 | 64.17 | 14.21 | 8.60 | 2.28 |
| | 5.0 | 94.47 | 63.49 | 12.59 | 5.74 | 2.32 |
| 22 | 3.0 | 94.77 | 65.43 | 17.23 | 11.58 | 2.20 |
| | 3.5 | 94.68 | 64.85 | 15.85 | 9.29 | 2.35 |
| | 4.0 | 94.58 | 64.18 | 14.22 | 6.26 | 2.28 |
| | 4.5 | 94.48 | 63.54 | 12.69 | 3.63 | 2.32 |
| | 5.0 | 94.37 | 62.79 | 10.92 | 0.39 | 0.39 |
| 24 | 3.0 | 94.69 | 64.89 | 15.92 | 7.19 | 2.23 |
| | 3.5 | 94.59 | 64.26 | 14.43 | 4.54 | 2.31 |
| | 4.0 | 94.48 | 63.53 | 12.67 | 1.20 | 1.20 |
| | 4.5 | - | - | - | - | - |
| | 5.0 | - | - | - | - | - |
| 26 | 3.0 | 94.79 | 58.35 | 8.37 | 6.29 | 2.19 |
| | 3.5 | 94.64 | 57.09 | 5.60 | 3.46 | 2.25 |
| | 4.0 | 94.45 | 55.64 | 2.40 | 0.18 | 0.18 |
| | 4.5 | - | - | - | - | - |
| | 5.0 | - | - | - | - | - |

From Table 11, the benchmark mix proportions for target void ratios in the range of 18% to 26% are obtained through theoretical calculations. Among these, the coarse

aggregate composition and amount requirements vary little with different void ratios. For target void ratios between 18% and 24%, the coarse aggregate composition and the resulting material void ratio are the same. However, for target void ratios greater than 24%, the material void ratio formed by the coarse aggregates will increase accordingly.

## 6. Mixing Processes of Porous Sustainable Mixtures

For asphalt mixtures, the sequence of material feeding, mixing temperature, and compaction method significantly affect their physical properties, mechanical performance, and serviceability [38]. In laboratory practice, commonly used compaction–molding methods include Marshall impact, static compaction, and gyratory compaction: gyratory compaction simultaneously applies vertical compression and horizontal shear, better simulating in situ kneading/rolling effects but requiring more complex and costly equipment [39]; Marshall impact is simple and reproducible, and in porous systems about 50 blows per side can form a stable aggregate skeleton, with 50 gyrations in an SGC producing specimens with similar volumetric characteristics [40,41]. For porous systems where sustainable epoxy resin replaces asphalt as the binder, strength arises mainly from resin curing; nevertheless, an appropriate feeding sequence, mixing temperature, and compaction method remain essential to ensure molding quality.

### *6.1. Sequence of Material Feeding*

For porous sustainable epoxy mixtures studied herein, the sequence of material feeding refers to the order in which the five categories of raw materials, coarse aggregates, fine aggregates, mineral filler, sustainable epoxy binder, and liquid polyurethane filler are introduced into the mixing process.

If the road-grade sustainable epoxy binder is first introduced into the mixing equipment, the binder or liquid polyurethane filler tends to adhere to the surface of the equipment, resulting in an actual binder content lower than the calculated value for laboratory-fabricated specimens, thereby affecting their volumetric properties and performance requirements. Similarly, if fine aggregates or mineral fillers are introduced first, due to their large specific surface area, subsequent direct addition of the sustainable epoxy binder may lead to agglomeration, causing non-uniform mixing and adversely affecting the mixture quality.

Furthermore, extensive laboratory trials have shown that, in order to ensure that the sustainable epoxy binder uniformly coats the surface of coarse aggregates, thus achieving desirable performance of porous sustainable epoxy resin mixtures, the sustainable epoxy binder should be added before the liquid polyurethane filler.

Accordingly, coarse aggregates should be fed first, with the sustainable epoxy binder added prior to the liquid polyurethane filler, while mineral filler should be added last. Based on this principle, two alternative feeding sequences were considered: First sequence: Coarse aggregates were added and mixed for 10 s, followed by fine aggregates (70 s), then the sustainable epoxy binder (70 s), liquid polyurethane filler (70 s), and finally mineral filler (70 s). Second sequence: Coarse aggregates were added and mixed for 10 s, followed directly by the sustainable epoxy binder (70 s), then liquid polyurethane filler (70 s), fine aggregates (70 s), and finally mineral filler (70 s).

For the skeleton–void type, aggregates were divided into coarse aggregates, fine aggregates, and mineral filler. Since mineral filler has a relatively large specific surface area and strong adsorption capacity toward the sustainable epoxy binder, it should be introduced last. Fine aggregates, with a surface area between that of coarse aggregates and mineral filler, may cause localized agglomeration if introduced prior to the sustainable

epoxy binder when binder content is relatively low, thereby hindering the formation of a uniform resin film on aggregate surfaces and weakening local adhesion.

It is hypothesized that mixtures prepared using the second feeding sequence would exhibit superior performance, since coarse aggregates are first introduced and mixed for 10 s, immediately followed by the introduction of the sustainable epoxy binder (70 s), ensuring a uniform resin film on the aggregate surface. Subsequent addition of liquid polyurethane filler, fine aggregates, and mineral filler promotes the formation of filler–binder mortar with the binder-coated coarse aggregates, avoiding localized non-uniformity and enhancing the performance of porous sustainable epoxy mixtures. In summary, within the laboratory conditions of this study, the feeding sequence for the porous sustainable epoxy mixtures is as follows: coarse aggregates → sustainable epoxy binder → liquid polyurethane filler → fine aggregates → mineral filler. The final feeding sequence is illustrated in Figure 9.

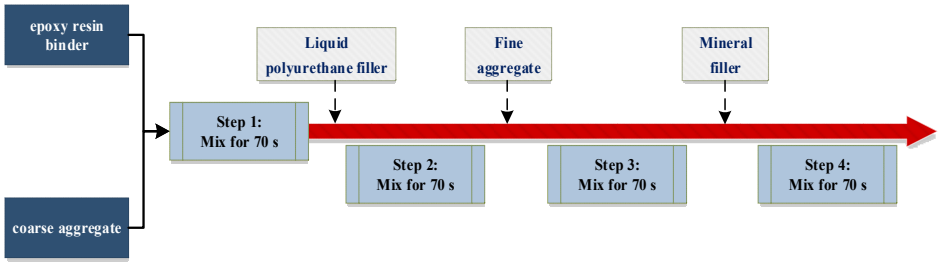


**Figure 9.** Feeding sequence of porous sustainable epoxy mixtures.

### *6.2. Mixing Temperature*

In the context of green, low-carbon development and the "dual-carbon" goals, the mixing temperature and molding process not only determine the volumetric and mechanical indices of asphalt mixtures but also directly affect construction energy use and carbon footprint. Ambient/low-temperature mixing can reduce the heating demand of aggregates and binder, thereby lowering energy consumption and greenhouse gas (GHG) and volatile organic compound (VOC) emissions, and improving the working environment. Within this framework, for asphalt mixtures, the asphalt binder is a viscoelastic material whose properties vary with temperature. Prior studies have shown that mixing, paving, and compaction temperatures during construction have significant influence on mixture performance. If the mixing temperature is improperly selected, it may lead to insufficient compaction, aging of the asphalt binder, and even aggregate crushing, thereby posing potential risks to pavement quality and service performance.

For porous sustainable epoxy mixtures, achieving an appropriate viscosity is crucial for uniform mixing and construction workability. This necessitates temperature control during mixing to obtain suitable viscosities for both the road-grade sustainable epoxy binder and the liquid polyurethane filler. The binder viscosities at different temperatures are measured using the Brookfield viscosity test, and the construction mixing temperature is determined based on the resulting viscosity–temperature relationship.

Laboratory mixing and compaction temperatures are commonly set by the equiviscous principle, and are usually about 0.17 ± 0.02 Pa·s for mixing and 0.28 ± 0.03 Pa·s for compaction. This approach can overestimate temperatures for polymer-modified binders due to shear-thinning, prompting alternative viscosity-based criteria [42]. In parallel, warm-mix asphalt (WMA) shows that lowering production temperatures by roughly 20–40 °C reduces fuel use and emissions while maintaining performance [43,44]. Building on these insights, our study defines a practical viscosity–temperature window for porous sustainable epoxy systems and verifies mixing uniformity, molding quality, and early-age performance, which are presented in Table 12 and Figure 10.

**Table 12.** Viscosity–temperature test results.

| Temperature (°C) | Viscosity (mPa·s) | |
|---|---|---|
| | Road-Grade Sustainable Epoxy Binder | Liquid Polyurethane Filler |
| 10 | 3700 | 37,000 |
| 15 | 2653 | 28,297 |
| 20 | 1600 | 19,667 |
| 25 | 1436 | 13,190 |
| 30 | 1280 | 6825 |
| 35 | 1190 | 5032 |
| 40 | 1100 | 3280 |
| 45 | 704 | 2378 |
| 50 | 305 | 1460 |
| 55 | 225 | 992 |
| 60 | 145 | 520 |

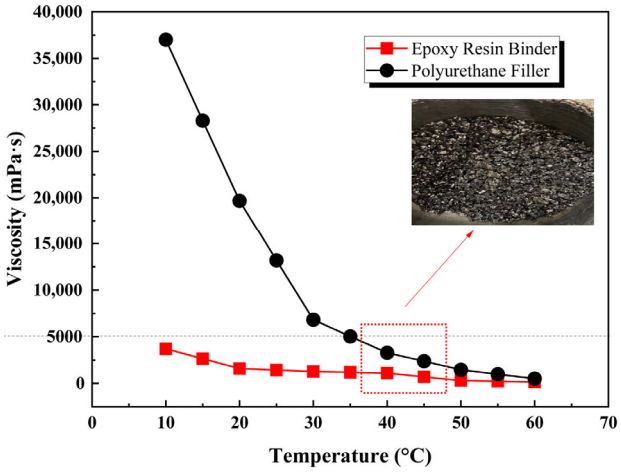


**Figure 10.** Viscosity–temperature curves for epoxy binder and liquid polyurethane filler.

As shown in Table 12, the viscosities of both the road-grade sustainable epoxy binder and the liquid polyurethane filler decrease markedly with increasing temperature. At lower temperatures, the sustainable epoxy binder exhibits viscosities far below those of the polyurethane filler; as temperature rises, the two values tend to converge. Therefore, the mixing temperature is a key parameter for achieving stable workability under laboratory conditions; however, the temperature window identified in this study should be verified and calibrated for plant-scale production conditions.

As shown in Figure 10, within the temperature range of 10–30 °C (exclusive of 30 °C), the sustainable epoxy binder viscosity remains below 8500 mPa·s, satisfying the basic viscosity requirement for mixing and permitting construction even in cold regions. By contrast, when the temperature is below 20 °C, the liquid polyurethane filler attains viscosities exceeding 19,667 mPa·s, which noticeably impair mixing uniformity and reduce construction efficiency.

In the higher-temperature range of 30–60 °C, the viscosities of the sustainable epoxy binder and polyurethane filler begin to converge. Based on extensive laboratory trials, when the mixing temperature is set to 30 °C, the viscosities of the sustainable epoxy binder and polyurethane filler are 1280 mPa·s and 6825 mPa·s, respectively, yielding mixtures with good uniformity. Accordingly, under hot summer conditions, conventional mixing can be employed without special temperature requirements; under colder climates, the mixing temperature may be appropriately increased, with 30 °C recommended.

## 7. Experimental Verifications of Sustainable Epoxy Mixture

The proposed baseline mix design method was validated experimentally. With the binder content fixed at 4.0%, the coarse aggregate gradation was computed from the target void ratio, and the corresponding fine aggregate and mineral filler were selected to assess the attainability and stability of the target void ratio. Experiments were conducted at target void ratios of 18%, 20%, 22%, 24%, and 26% to determine void volume characteristics, scattering resistance, permeability, and mechanical properties. The evaluation, under the fixed-binder condition, examined the method's control over mixture composition and key pavement performance and delineated its range of applicability.

### *7.1. Void Volume Characteristics*

Figure 11 presents the measured void ratios for different target void ratios at a binder content of 4.0%.

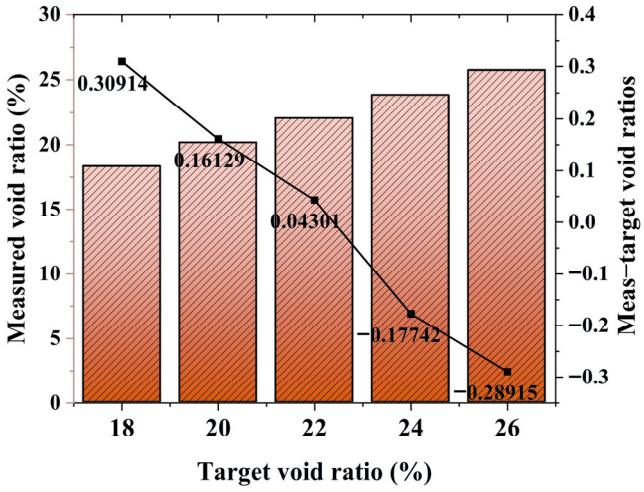


**Figure 11.** Comparison of measured void ratios for different mixtures.

From Figure 11, under a binder content of 4.0%, the measured void ratio increases sequentially as the target void ratio rises from 18% to 26%, and the two exhibit approximately linear correspondence. In the baseline mix-proportion calculation, mixtures with different binder contents are determined based on the target void ratio and the reserved void method. The observed change in measured void ratio may be attributed to the fact that increasing the binder content reduces interparticle friction among coarse aggregates; under the same compaction energy, the aggregate particles can rearrange more readily, producing a denser mixture and thus a lower void ratio.

Figure 11 also shows how the difference between the measured and target void ratios varies with binder content. At a binder content of 4.0%, the deviation between the measured and target void ratios is within ±0.4%, indicating that the baseline mix proportion determined in this study meets the target void ratio requirement and satisfies the accuracy needed for engineering design.

### *7.2. Abrasion Resistance*

The Cantabro abrasion test results for the mixtures are shown in Figure 12. For porous epoxy resin mixtures with a binder content of 4.0% at different target void ratios, the scattering loss rate ranges from 4.95% to 9.63%, meeting the requirement in the porous asphalt mixture specification that the scattering loss rate be less than 15%.

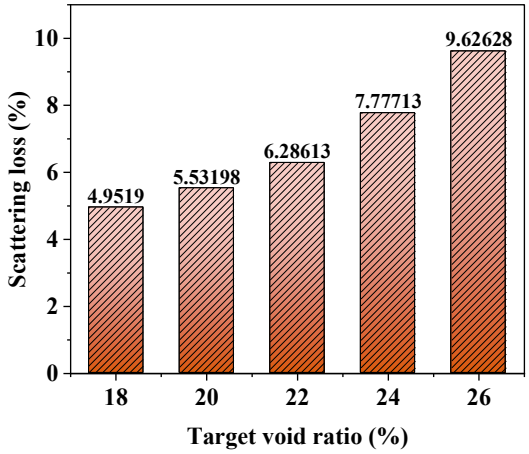


**Figure 12.** Variation in scattering loss with target void ratio for different mixtures.

For mixtures with the same binder content, a higher target void ratio corresponds to a higher scattering loss rate, indicating a greater tendency for scattering loss. Specifically, at a binder content of 4.0%, as the target void ratio increases from 18% to 26%, the scattering loss rate rises from 4.95% to 9.63%, i.e., by 4.68 percentage points. This may be because mixtures with larger target void ratios have a more open internal void structure, resulting in smaller contact areas between aggregate particles and weaker interparticle bonding.

### *7.3. Permeability*

To quantify how target air-void content and total binder dosage influence permeability, constant-head tests were performed on mixtures with target air-void contents of 18% to 26% at a binder dosage of 4.0%. Results are summarized in Figure 13.

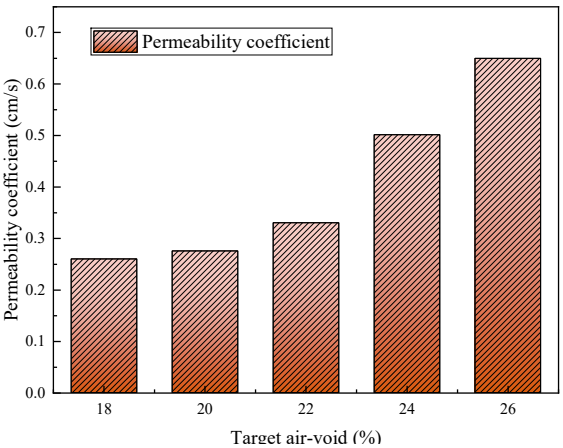


**Figure 13.** Permeability coefficient versus target air-void content.

As illustrated in Figure 13, the permeability coefficient increases from 0.26 cm/s at 18% voids to 0.33 cm/s at 22% and 0.65 cm/s at 26%. The increment from 18% to 22% is modest ($\Delta k$ = 0.07 cm/s), whereas from 22% to 26% the increase is pronounced ($\Delta k$ = 0.32 cm/s). Hence, when the target air-void content is below ~22%, permeability changes little with voids; beyond ~22%, hydraulic conductivity rises sharply. Substituting epoxy resin for asphalt to produce ultra-high-void epoxy mixtures is therefore highly beneficial for drainage functionality.

### *7.4. Mechanical Properties*

#### 7.4.1. Uniaxial Compression

Load–displacement responses of vertical displacement are shown in Figure 14.

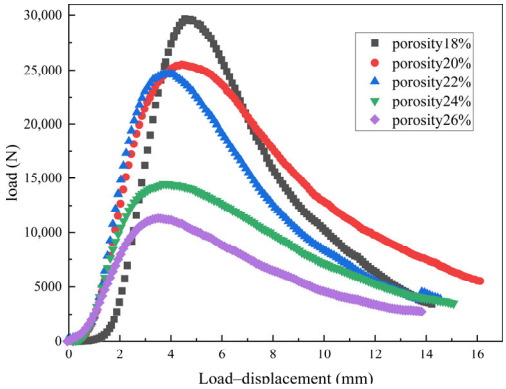


**Figure 14.** Load–displacement curves under uniaxial compression.

Overall, mixtures with different target voids exhibit a similar trend: load increases and then decreases with displacement; after the peak, the load drops gradually rather than abruptly, indicating non-brittle failure and residual load-bearing capacity. Higher target voids lead to lower peak loads but better deformation coordination. For a fixed binder dosage, larger void contents imply relatively more binder at coarse aggregate contacts, strengthening interparticle bonding and improving coordinated deformation.

As illustrated in Table 13, compressive strength declines with increasing target voids, and this sensitivity is amplified at higher binder dosages. Under the baseline mix design, greater void contents correspond to a less stable coarse aggregate skeleton, reducing strength; in addition, higher binder dosages thicken the binder film on aggregate surfaces, further increasing skeleton instability and its sensitivity to voids. For porous epoxy mixtures, the failure-load displacement falls within 3.49–4.54 mm, and the resilient modulus within 193.10–595.30 MPa. By comparison, porous asphalt mixtures typically fail at 2–3 mm of displacement, with a resilient modulus $\geq$ 700 MPa. Thus, porous epoxy mixtures display superior deformation coordination under load relative to porous asphalt.

**Table 13.** Uniaxial compression results.

| Target Air Void/% | Max. Load/kN | Displacement at Max. Load/mm | Compressive Strength/MPa | Resilient Modulus/MPa |
|---|---|---|---|---|
| 18 | 29.68 | 4.55 | 3.78 | 595.30 |
| 20 | 25.54 | 4.42 | 3.52 | 451.00 |
| 22 | 24.69 | 4.04 | 3.15 | 359.54 |
| 24 | 14.47 | 3.71 | 1.84 | 280.58 |
| 26 | 11.32 | 3.50 | 1.44 | 193.10 |

As target voids increase, both the failure-load displacement and the resilient modulus decrease. For example, at 4% binder dosage, raising target voids from 18% to 22% reduces the failure-load displacement from 4.55 to 3.50 mm (−1.05 mm) and the resilient modulus from 595.30 to 193.10 MPa (−302.20 MPa). Hence, higher void contents make mixtures more failure-prone under loading, yet before failure, they exhibit markedly improved coordinated deformation. Mechanistically, higher-void mixtures possess a more open internal structure and altered contact states within the coarse aggregate skeleton; for the same binder dosage, larger voids produce a thicker binder film on aggregate surfaces, enhancing coordinated

deformation prior to failure. The pavement-grade epoxy resin employed here shows an elongation at break exceeding 100% at room temperature, reflecting good toughness. Consequently, replacing conventional asphalt with epoxy as the binder yields porous mixtures that combine relatively high strength with excellent deformation coordination.

#### 7.4.2. Splitting (Indirect Tensile) Strength

The experimental results are shown in Figure 15, highlighting that the splitting strength of porous epoxy mixtures ranges from 0.25 to 0.53 MPa, comparable to that of porous asphalt. For a fixed binder dosage, strength decreases with increasing target voids: raising voids from 18% to 26% reduces strength from 0.52 to 0.25 MPa (−0.27 MPa), confirming the strong influence of air-void content on ITS.

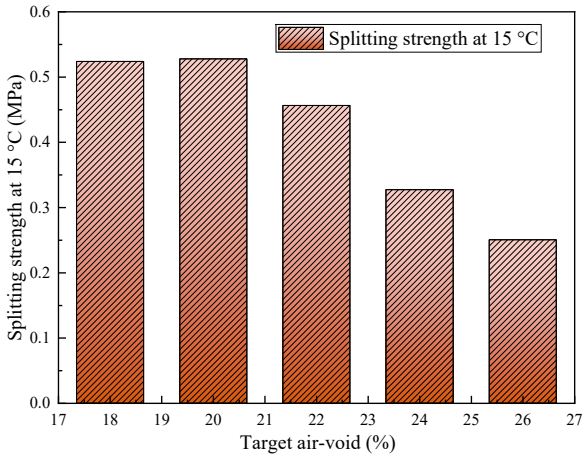


**Figure 15.** Splitting test results at 15 °C.

#### 7.4.3. Correlation Analysis

To systematically elucidate the intrinsic correlations among macroscopic mechanical indicators and identify the governing structural parameters, Pearson correlation analysis was performed on the experimental data from uniaxial compression and splitting tensile tests. The analysis encompassed the target air void, displacement at maximum load, compressive strength, resilient modulus, and splitting tensile strength. By constructing a linear correlation matrix, the interdependences and mutual interactions among these variables were quantitatively evaluated. This statistical approach reveals the coupled relationships between the material's deformation behavior, stiffness characteristics, and strength performance. The resulting correlation matrix is summarized in Table 14.

**Table 14.** Correlation analysis between uniaxial compression testing and splitting tests.

| | Target Air Void | Displacement at Max Load | Compressive Strength | Resilient Modulus | Splitting Strength |
|---|---|---|---|---|---|
| Target air void | 1 | −0.99044 | −0.96342 | −0.99211 | −0.94997 |
| Displacement at max load | −0.99044 | 1 | 0.97478 | 0.9707 | 0.96985 |
| Compressive strength | −0.96342 | 0.97478 | 1 | 0.93036 | 0.98838 |
| Resilient modulus | −0.99211 | 0.9707 | 0.93036 | 1 | 0.90412 |
| Splitting strength | −0.94997 | 0.96985 | 0.98838 | 0.90412 | 1 |

Pearson correlation analysis reveals a highly consistent and physically significant structure among the investigated parameters. With absolute correlation coefficients ($|r|$) predominantly exceeding 0.90, the system exhibits robust linear interdependencies.

First, the target air void serves as a primary determinant, showing strong negative correlations with all mechanical indicators. Specifically, the target air void correlates al-

most linearly with displacement at maximum load (r = −0.990) and resilient modulus (r = −0.992), indicating that pore expansion severely degrades material stiffness and deformation resistance. Similar trends are observed for compressive (r = −0.963) and splitting tensile strengths (r = −0.950), suggesting that higher porosity disrupts the continuity of the load-bearing skeleton and impedes stress transfer pathways.

Furthermore, displacement at maximum load positively aligns with strength and stiffness metrics (r: 0.970–0.975), signifying a synergy between ultimate deformation capacity and macroscopic load-bearing behavior. Notably, the correlation between compressive and splitting tensile strengths reaches 0.988, underscoring the dominant role of structural compactness across different loading modes. Although slightly lower (r > 0.90), the correlation between resilient modulus and strength confirms a stable coupling between material stiffness and resistance.

In summary, the target air void is the key governing parameter for macroscopic performance, while strength, stiffness, and deformation indices exhibit a synchronized evolutionary pattern. These findings validate the internal consistency of the experimental data and provide a robust statistical foundation for developing predictive models based on void structures.

### *7.5. High-Temperature Stability*

As illustrated in Table 15, the dynamic stability of the porous epoxy resin mixtures, when utilizing a 4.0% binder content across various target void ratios, ranged between 45,000 and 90,000 cycles/mm. This range demonstrates a significant enhancement in rutting resistance when compared to conventional porous asphalt mixtures.

**Table 15.** Rutting test results for various mixtures.

| Binder Content (%) | Target Void Ratio (%) | Deformation (45 min) | Deformation (60 min) | Dynamic Stability (Cycles/min) |
|---|---|---|---|---|
| 4.0 | 18 | 0.213 | 0.22 | 90,000 |
| | 20 | 0.322 | 0.330 | 78,750 |
| | 22 | 0.269 | 0.279 | 63,000 |
| | 24 | 0.491 | 0.503 | 52,500 |
| | 26 | 0.381 | 0.395 | 45,000 |

Specifically, the mixture designed with a 26% target void ratio and a 4% binder content exhibited the minimum dynamic stability, recorded at 45,000 cycles/mm. This value substantially surpasses the requirement of 3000 cycles/mm stipulated for modified Stone Mastic Asphalt (SMA) mixtures in the Technical Specification for Construction of Highway Asphalt Pavements (JTG F40-2004) [45].

Furthermore, for mixtures prepared with an identical binder content, a decrease in the target void ratio leads to a proportional increase in the dynamic stability of the mixture. This correlation is attributed to the reduced void ratio, which necessitates a relative increase in the internal components, including the composite binder, fine aggregate, and mineral filler. The resulting greater compaction and density of the mixture, after curing the binder, subsequently yield superior high-temperature rutting resistance.

### *7.6. Resistance to Low-Temperature Cracking*

The results of the splitting tests performed at −10 °C are illustrated in Figure 16.

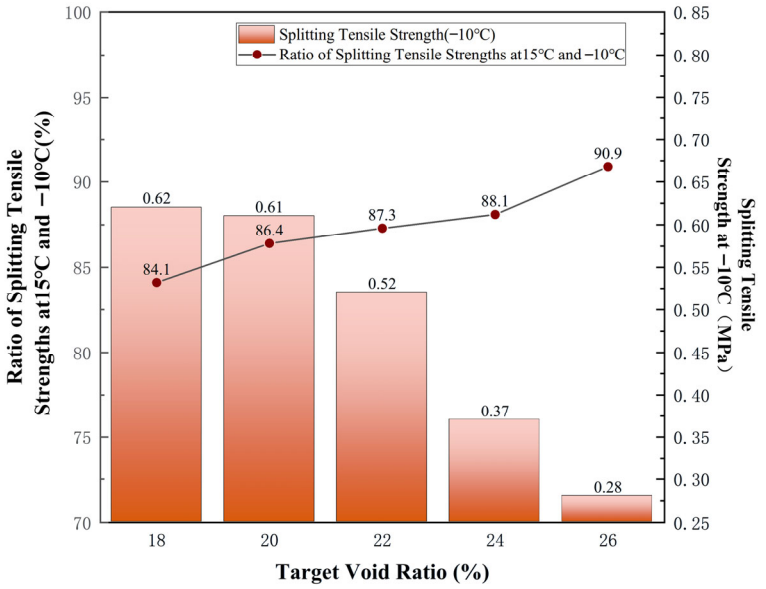


**Figure 16.** Splitting tensile strength and splitting tensile strength ratio.

It is evident from Figure 16 that, under the thermal condition of −10 °C, the splitting tensile strength of the various mixtures ranges from 0.28 MPa to 0.62 MPa, a range that is lower than the low-temperature splitting strength typically observed for porous asphalt mixtures.

A general trend was initially observed that a smaller target void ratio corresponded to a higher −10 °C splitting tensile strength. However, when the binder content was maintained at 4%, reducing the target void ratio from 26% to 18% was associated with a decrease in the mixture's −10 °C splitting tensile strength, specifically dropping from 0.62 MPa to 0.28 MPa, a substantial reduction of 0.34 MPa. This significant magnitude of variation clearly underscores the profound influence of the target void ratio on the low-temperature splitting performance of the mixture. This phenomenon can be primarily attributed to the expansion of the target void ratio, which progressively enlarges the skeletal voids within the mixture. Consequently, the diminished contact area among the coarse aggregates compromises the cohesive and bonding efficacy of the hybrid binder.

Furthermore, the resulting ratio of the splitting tensile strengths between 15 °C and −10 °C was observed to fall within the range of 80% to 100%. This suggests that, following the reduction in temperature, the splitting tensile strength of the mixture did experience a slight increase, yet the overall change was not highly pronounced. This stability can be ascribed to the favorable low-temperature characteristics of the hybrid binder employed in the present investigation, which can guarantee a cross-sectional elongation capacity of 60% to 80% even under the −10 °C test condition.

## 8. Conclusions

This study systematically collects and synthesizes existing research findings on the gradation of porous asphalt concrete (PAC) materials. By employing statistical approaches, the relationship between the target void ratio and the gradation distribution of aggregates is examined, with particular emphasis on establishing the correlation between the gradation composition and the desired void ratio. The principal research conclusions are as follows:

(1) Through statistical analysis of the relationship between the sieve passing rates of aggregate materials and the void ratio, it is identified that the 2.36 mm sieve serves as the critical boundary between coarse and fine aggregates, exhibiting the strongest correlation with the void ratio. Consequently, the passing rates of the 2.36 mm and

4.75 mm sieves must be carefully controlled during mix-proportion design to ensure optimal gradation and performance.

(2) Through mathematical statistics, theoretical calculations, and related methods, the relationships among the target void ratio, binder mixture, and material gradation composition were established. Specifically, the amounts of other coarse aggregates were first calculated based on the prescribed target void ratio and the dosage of 13.2 mm coarse aggregate. Subsequently, filling tests were employed to derive a multiple linear relationship between the material void ratio and the sieve residue of different coarse aggregate fractions. Furthermore, according to the theory of compaction packing, mineral filler was simplified as spherical particles with an average diameter of 0.075 mm, which was used to estimate the quantity of mineral powder required to envelop the surface of the coarse aggregates.

(3) Based on the void-filling theory, the total volume of target void ratio, fine aggregates, mineral powder, and binder mixture was controlled to equal the void volume within the compacted coarse aggregate skeleton. This approach allowed for the determination of the appropriate quantities of fine aggregates, mineral powder, and binder mixture, thereby establishing a method for calculating the benchmark mix proportion for different target void ratios and binder mixture contents.

(4) This study confirmed that the mixing sequence, compaction method, and mixing temperature were critical parameters governing the preparation of porous sustainable mixtures. Laboratory verification demonstrated that sequentially adding coarse aggregate, sustainable epoxy binder, liquid polyurethane filler, fine aggregate, and mineral filler at 30 °C, followed by 50 double-sided blows, produced well-compacted specimens and established a reliable protocol for mixture fabrication.

(5) Viscosity–temperature analysis demonstrated that temperature was the primary determinant of stable workability in porous sustainable mixtures. At low temperatures, the polyurethane filler dominated the rheology, limiting dispersion, whereas a controlled moderate mixing temperature generated a modest and advantageous viscosity contrast between phases, enhancing binder coating, aggregate interlocking, and pore retention. Accordingly, systematic temperature control of the mixture, particularly the polyurethane component, combined with in-process consistency checks, was essential to achieve uniform mixing, reliable compaction, and reproducible void structures across different climatic conditions.

(6) Experimental verification under the proposed framework indicated that, at a binder content of 4.0%, the deviation between measured and target void ratios was within ±0.4%. For target void ratios of 18–26%, Cantabro loss ranged from 4.95% to 9.63% (<15%), and the permeability coefficient increased from 0.26 cm/s (18%) to 0.65 cm/s (26%). Mechanical results showed that compressive strength decreased from 3.78 MPa to 1.44 MPa as void ratio increased from 18% to 26%, while ITS at 15 °C ranged from 0.25 to 0.53 MPa. Rutting resistance remained high, with dynamic stability ranging from 45,000 to 90,000 cycles/mm at a binder content of 4.0%. At 30 °C, the viscosities of the sustainable epoxy binder and polyurethane filler were 1280 mPa·s and 6825 mPa·s, respectively, corresponding to improved mixing uniformity under laboratory conditions.

This study establishes and verifies the proposed framework based on the PAC-13 mixture with the epoxy resin binder system. Extending the framework to other NMAS PAC gradations (e.g., PAC-16) and/or different aggregate sources/types (including recycled aggregates) requires rebuilding the statistical gradation dataset, updating material inputs (e.g., density, absorption, and morphology), and recalibrating and verifying the

model coefficients. It is also suggested to investigate its long-term field performance in future work.

**Author Contributions:** Conceptualization, G.Z. and B.M.; methodology, G.Z., B.N., T.G., and B.M.; formal analysis, G.Z., B.N., and F.C.; investigation, G.Z., T.L., S.G., T.G., and R.W.; resources, B.M.; data curation, G.Z. and S.G.; writing—original draft preparation, G.Z., B.N., F.C., T.L., and S.G.; writing—review and editing, T.G., B.M., and R.W.; supervision, B.M.; project administration, B.M.; funding acquisition, B.M. All authors have read and agreed to the published version of the manuscript.

**Funding:** This research was funded by the CCCC-SHEC Seventh Highway Engineering Co., Ltd. under the grant numbers 220221230584, 220221230594, and 220221230552.

**Institutional Review Board Statement:** Not applicable.

**Informed Consent Statement:** Not applicable.

**Data Availability Statement:** Data will be made available on request.

**Conflicts of Interest:** Authors Genhe Zhang, Bo Ning, Feng Cao and Taotao Li were employed by China Communications Second Highway Engineering Bureau 7th Co., Ltd. Author Teng Gao was employed by Xi'an Highway Survey and Design Institute Co., Ltd. Author Biao Ma have received research grants from Company CCCC-SHEC Seventh Highway Engineering Co., Ltd. The remaining authors declare that the research was conducted in the absence of any commercial or financial relationships that could be construed as a potential conflict of interest.

## Abbreviations

The following abbreviations are used in this manuscript:

| | |
|---|---|
| PAC | Permeable Asphalt Concrete |
| WMA | Warm-mix asphalt |
| SMA | Stone Mastic Asphalt |
| CAVF | Coarse aggregate void-filling method |
| SGC | Superpave Gyratory Compactor |
| RD | Rut Depth |
| DS | Dynamic stability |
| VMA | Voids in mineral aggregate |
| VCA* | Coarse aggregate material void ratio |
| VV | Target void ratio |
| GHG | Greenhouse gas |
| VOC | Volatile organic compound |
| $A_{13.2}$ | Sieve residue for the 13.2 mm sieve fraction |
| $A_{9.5}$ | Sieve residue for the 9.5 mm sieve fraction |
| $A_{4.75}$ | Sieve residue for the 4.75 mm sieve fraction |
| $A_{2.36}$ | Sieve residue for the 2.36 mm sieve fraction |

## References

1. Kang, X.; Zhang, B.; Yin, Y.; Hu, Y.; Wang, X.; Si, W. Progress in research on the mechanisms of clogging behavior and its influencing factors in porous asphalt pavements. *Constr. Build. Mater.* **2025**, *501*, 144324. [CrossRef]
2. Li, B.; Zhao, H.; Zhou, J.; Yao, T.; Guo, F.; Hu, Y. Investigation on sound absorption coefficients of porous asphalt concrete under different clogging conditions. *Constr. Build. Mater.* **2024**, *428*, 136081. [CrossRef]
3. Hu, Y.; Yin, Y.; Sreeram, A.; Liu, J.; Si, W.; Tang, D.; Airey, G.D. Nano-aggregation of asphaltenes and its influence on the multiscale properties of bitumen recycled through multiple ageing and rejuvenation cycles. *Chem. Eng. J.* **2025**, *512*, 162348. [CrossRef]
4. Patel, D.; Jahan, H.; Hu, Y.; Hejazi, S.; Roja, K.L.; Airey, G.; Sreeram, A. Incorporating bio-based lignin as a sustainable fine aggregate in asphalt mixtures: Comprehensive analysis of long-term performance. *Sustain. Mater. Technol.* **2025**, *46*, e01734. [CrossRef]

5. Hu, Y.; Wang, H.; Zhou, L.; Airey, G.D. Towards an enhanced understanding of the functional groups within bitumen during ageing processes. In *Advances in Functional Pavements*; CRC Press: Boca Raton, FL, USA, 2024; pp. 83–87.
6. Omairey, E.; Hughes, D.; Hu, Y.; Airey, G. Feasibility evaluation of bio-waste derived, plastic-waste modified binder rejuvenators. In *Advances in Functional Pavements*; CRC Press: Boca Raton, FL, USA, 2024; pp. 58–61.
7. Wang, X.; Ma, B.; Yu, M.; Mao, W.; Si, W. Testing and modeling of incomplete phase change heat storage and release of epoxy resin/microcapsule composite phase change materials for asphalt pavement. *J. Energy Storage* **2025**, *105*, 114672. [CrossRef]
8. Li, B.; Zhang, Y.; Wei, D.; Yao, T.; Hu, Y.; Dou, H. Evolution of clogging of porous asphalt concrete in the seepage process through integration of computer tomography, computational fluid dynamics, and discrete element method. *Comput. Aided Civ. Infrastruct. Eng.* **2025**, *40*, 1652–1674. [CrossRef]
9. Ren, S.; Liu, X.; Erkens, S. Insight into the critical evaluation indicators for fatigue performance recovery of rejuvenated bitumen under different rejuvenation conditions. *Int. J. Fatigue* **2023**, *175*, 107753. [CrossRef]
10. Li, H.; Luan, Y.; Sun, Q.; Ma, T.; Xu, M.; Li, Y. Quantitative evaluation of fatigue damage behavior of recycled asphalt mixture based on tensile and compressive anisotropy. *Constr. Build. Mater.* **2025**, *484*, 141842. [CrossRef]
11. Hu, Y.; Yin, Y.; Sreeram, A.; Si, W.; Airey, G.D.; Li, B.; Singh, B.; Kaya Özdemir, D.; Zhou, L. Atomic Force Microscopy (AFM) based microstructural and micromechanical analysis of bitumen during ageing and rejuvenation. *Constr. Build. Mater.* **2025**, *467*, 140387. [CrossRef]
12. Hu, Y.; Sreeram, A.; Bahia, H.U.; Airey, G.D.; Si, W.; Li, B.; Xu, X. Assessing correlations between two linear amplitude sweep (LAS) standards for evaluating the fatigue properties of aged bitumen. *Int. J. Pavement Eng.* **2024**, *25*, 2375419. [CrossRef]
13. Zhou, S.; Long, K.; Zhang, Z.; Li, S.; Ai, C.; Yan, C. Development of sustainable Lignin-Based coatings for layered double Hydroxides: Enhancing synergistic Anti-Aging properties in bitumen. *Fuel* **2025**, *380*, 133166. [CrossRef]
14. Ren, S.; Zhang, Y.; Pipintakos, G.; Xu, S.; Liu, Q.; van den Bergh, W. Elucidating the role of lignin in bio-rejuvenated bitumen: Insights into rheological and anti-aging properties via experiments and molecular simulations. *Fuel* **2025**, *395*, 135244. [CrossRef]
15. Si, W.; Xia, M.; Zhang, B.; Danzeng, G.A.; Wang, X.; Hu, Y.; Li, X.; Zhong, M.; Yin, Y. Study on the preparation and performance optimization of wear-resistant asphalt pavement composite functional material reflective cooling coatings. *Const. Build. Mater.* **2026**, *508*, 145055. [CrossRef]
16. Xiang, Q.; Xiao, F. Applications of epoxy materials in pavement engineering. *Constr. Build. Mater.* **2020**, *235*, 117529. [CrossRef]
17. Liu, X.; Wu, Z.; Min, Z.; Zhang, L. Investigation on the Preparation and Performances of Epoxy-Modified Asphalt Binder and Its Mixtures. *Materials* **2024**, *17*, 2539. [CrossRef]
18. Ma, B.; Wei, K.; Huang, X.F.; Shi, W.S.; Chen, S.S.; Hu, Y.P.; Shi, H.T. Preparation and Investigation of NiTi Alloy Phase-Change Heat Storage Asphalt Mixture. *J. Mater. Civ. Eng.* **2020**, *32*, 04020250. [CrossRef]
19. Ma, B.; Hu, Y.; Si, W.; Wei, K.; Chang, X. Study on the temperature control effects of an epoxy resin composite thermoregulation agent on asphalt mixtures. *Constr. Build. Mater.* **2020**, *257*, 119580. [CrossRef]
20. Liu, P.; Sheng, X.Y.; Li, L.; Hao, Z.H. Influence of toughened epoxy resin dosage on performance of asphalt mixture. *New Chem. Mater.* **2019**, *47*, 245–248.
21. Xu, J.; Ma, B.; Mao, W.; Wang, X.J.C.; Materials, B. Strength characteristics and prediction of epoxy resin pavement mixture. *Constr. Build. Mater.* **2021**, *283*, 122682. [CrossRef]
22. Du, J.; Mahjoubi, S.; Bao, Y.; Banthia, N.; Meng, W.A. Modeling mixing kinetics for large-scale production of Ultra-High-Performance Concrete: Effects of temperature, volume, and mixing method. *Constr. Build. Mater.* **2023**, *397*, 132439. [CrossRef]
23. Kisku, N.; Rajhans, P.; Panda, S.K.; Pandey, V.; Nayak, S. Microstructural investigation of recycled aggregate concrete produced by adopting equal mortar volume method along with two stage mixing approach. *Structures* **2020**, *24*, 742–753. [CrossRef]
24. Li, Z.X.; Wang, X.; Zhu, Z.G.; Wu, Z.S. Effect of mixing methods on the dispersion of fibers in the gypsum matrix and performance improvement mechanism. *Constr. Build. Mater.* **2022**, *320*, 126193. [CrossRef]
25. El-Mir, A.; Fayad, E.; Assaad, J.J.; El-Hassan, H. Multi-Response Optimization of Semi-Lightweight Concrete Incorporating Expanded Polystyrene Beads. *Sustainability* **2023**, *15*, 8757. [CrossRef]
26. *GB/T 2567-2021*; Test Methods for Properties of Resin Casting Body. Chinese National Standard: Beijing, China, 2021.
27. Chen, J.; Li, H.; Wang, L.B.; Wu, J.T.; Huang, X.M. Micromechanical characteristics of aggregate particles in asphalt mixtures. *Constr. Build. Mater.* **2015**, *91*, 80–85. [CrossRef]
28. *JTG 3410-2025*; Standard Test Methods of Asphalt and Asphalt Mixture for Highway Engineering. Research Institute of Highway Ministry of Transport: Beijing, China, 2025.
29. *JTG/T 3350-03-2020*; Design and Construction of Drainage Asphalt Pavements. Ministry of Transport of the People's Republic of China: Beijing, China, 2020.
30. Hansen, K. *Porous Asphalt Pavements for Stormwater Management: Design, Construction, and Maintenance Guide*; National Asphalt Pavement Association: Greenbelt, MD, USA, 2008.
31. Texas Department of Transportation. *Standard Specifications for Construction and Maintenance of Highways, Streets, and Bridges: Adopted by the Texas Department of Transportation, November 1, 2014*; Texas Department of Transportation: Austin, TX, USA, 2014.

32. FHWA. *Porous Asphalt Pavements with Stone Reservoirs*; FHWA: Washington, DC, USA, 2015.
33. Jun, Y.; Fen, Y.; Peng, H.; Yirong, W.; Ping, S. Evaluation on Permeability of Porous Asphalt Mixture. *J. Highw. Transp. Res. Dev.* **2002**, *19*, 35–37+40.
34. Slebi-Acevedo, C.J.; Lastra-González, P.; Indacoechea-Vega, I.; Castro-Fresno, D. Development of improved porous asphalt mixtures with high porosity levels. *Dev. Built Environ.* **2023**, *16*, 100286. [CrossRef]
35. Ghuzlan, K.A.; Bara'W, A.-M.; Al-Momani, A.S. Rutting performance of asphalt mixtures with gradations designed using Bailey and conventional Superpave methods. *Constr. Build. Mater.* **2020**, *261*, 119941. [CrossRef]
36. Wang, L.; Ma, B.; Kou, J.-P. Gradation design method of coarse aggregate for interlocking-dense cement concrete. *J. Traffic Transp. Eng.* **2011**, *11*, 12–17.
37. Suo, Z.; Bao, X.; Nie, L.; Yan, Q.; Qi, K. Optimization Design of Mix Proportion of Large Stone Permeable Mixture Based on Target Air Voids. *Buildings* **2021**, *11*, 514. [CrossRef]
38. Si, W.; Zhang, B.; Zhang, X.; Xia, W.; Cheng, X.; Luo, X.; Hu, Y. Maximizing the circularity of asphalt pavements by improving the RAP content in recycled asphalt mixtures. *Constr. Build. Mater.* **2024**, *438*, 137316. [CrossRef]
39. Cai, X.; Li, X.; Wu, K.-H.; Huang, W.-K. Grading Design of Recycled Aggregate Cement-stabilized Gravel Based on Rotary Compaction. *J. Highw. Transp. Res. Dev. Engl. Ed.* **2018**, *12*, 1–6. [CrossRef]
40. Li, J.G.; Sha, A.M.; Jiang, W.; Liu, Z.Z.; Jia, M.; Han, Z.Q. Study on dynamic responses of particle in aggregate mixture during the laboratory compaction utilizing Smart Aggregate. *Constr. Build. Mater.* **2022**, *344*, 128156. [CrossRef]
41. Sha, A.M.; Ren, X.Y.; Li, J.E.; Jiang, W.; Jia, M. Densification behavior of asphalt mixture and its relation with particle dynamic responses during gyratory compaction. *Constr. Build. Mater.* **2023**, *377*, 131138. [CrossRef]
42. Liu, Z.; Liu, Z.; Huang, Y.; Cao, Y. Determining the Compaction Temperature of Warm-Mix Anti-Rutting Asphalt Mixture. *Appl. Sci.* **2024**, *14*, 11042. [CrossRef]
43. Milad, A.; Babalghaith, A.M.; Al-Sabaeei, A.M.; Dulaimi, A.; Ali, A.; Reddy, S.S.; Bilema, M.; Yusoff, N.I.M. A Comparative Review of Hot and Warm Mix Asphalt Technologies from Environmental and Economic Perspectives: Towards a Sustainable Asphalt Pavement. *Int. J. Environ. Res. Public Health* **2022**, *19*, 14863. [CrossRef] [PubMed]
44. Rathore, M.; Haritonovs, V.; Zaumanis, M. Performance Evaluation of Warm Asphalt Mixtures Containing Chemical Additive and Effect of Incorporating High Reclaimed Asphalt Content. *Materials* **2021**, *14*, 3793. [CrossRef]
45. *JTG F40-2004*; Technical Specifications for Construction of Highway Asphalt Pavements. Industry Standard of China: Beijing, China, 2004.